G.A. Wilhold ED31

LMSC-HEC TR F268519

TECHNICAL REPORT

TURBINE ROTOR/STATOR FLOWFIELD ANALYSIS

March 1989

Contract NAS8-36284

Prepared for

NATIONAL AERONAUTICS AND SPACE ADMINISTRATION
GEORGE C. MARSHALL SPACE FLIGHT CENTER
MARSHALL SPACE FLIGHT CENTER, AL 35812

by

Lisa Griffin

Lockheed
Missiles & Space Company, Inc.
Huntsville Engineering Center
4800 Bradford Blvd., Huntsville, AL 35807

FOREWORD

This report documents numerical results obtained by personnel of the Computational Mechanics Section at Lockheed's Huntsville Engineering Center under Contract NAS8-36284, "Turbine Rotor/Stator Flowfield Analysis."

The NASA-MSFC Contracting Officer's Representative for this study is Dr. Helen V. McConnaughey, ED32.

ABSTRACT

A numerical study of the unsteady aerodynamic and thermal environment associated with axial turbine stages is presented. Computations are performed using a modification of the ROTOR1 rotor/stator interaction code developed by M.M. Rai. Two different turbine stages are analyzed: the first stage of the United Technologies Research Center large scale rotating rig and the first stage of the Space Shuttle main engine (SSME) high pressure fuel turbopump. Time-averaged blade midspan pressure and heat transfer profiles are calculated using the following different surface boundary conditions: adiabatic wall, prescribed wall temperature, and prescribed heat flux. Numerical solutions for the large scale rotating rig are compared with experimental data. Unsteady pressure envelopes are also presented for each geometry. In addition, instantaneous contours are plotted for the SSME configuration.

CONTENTS

CONTENTS (Concluded)

LIST OF FIGURES

LIST OF SYMBOLS

a	speed of sound
C	chord
C_p	coefficient of pressure
c_p	specific heat, constant pressure
c_v	specific heat, constant volume
J	Jacobian of coordinate transformation
K	coefficient of thermal conductivity
M	Mach number
p	pressure
q"	heat flux
St	Stanton number
T	temperature
U	velocity magnitude
u,v	x and y components of velocity
X	axial distance
Y^+	boundary layer parameter
μ	coefficient of viscosity
ρ	density
ω	rotor speed

Subscripts

a	adiabatic conditions
e	exit condition
new	condition for revised quantities in iteration procedure
old	current (unrevised) quantities in iteration procedure
T	total (stagnation) quantity
w	wall condition
0	inlet condition
2	quantity at first row of nodes off boundary

1. INTRODUCTION

Current propulsion systems demand optimal performance and increased blade durability. To meet these demands, a clear understanding is needed of the unsteady aerodynamic and thermal environment associated with turbomachinery. In the past few years, turbine analysis capabilities have been enhanced through the development of computational fluid dynamics (CFD) codes that solve for the unsteady viscous flowfield in an axial turbine stage. The objective of this work is to extend and further evaluate the unsteady codes. Predictive capability is assessed in terms of the accuracy of calculated aerodynamic and thermal blade loads and in terms of suitability for rocket propulsion applications.

Specifically, ROTOR1, an unsteady rotor/stator interaction code, was modified to include heat transfer prediction capability. The original ROTOR1 (an adiabatic wall version) and the modified ROTOR1 (a prescribed wall temperature or prescribed heat flux version) were applied to the midspan of two different turbine stages: the first stage of the United Technologies Research Center (UTRC) large scale rotating rig (LSRR) (for which tests were performed and reported in Refs. 1, 2, and 3) and the Space Shuttle main engine (SSME) high pressure fuel turbopump (HPFTP) turbine first stage. Results are presented in the form of time-averaged blade pressure coefficients and heat transfer coefficients. All results obtained for the LSRR are compared with experimental data. In addition, time-varying flow features are also presented.

2. CONFIGURATIONS AND CONDITIONS

The turbine stage flows analyzed in this study are described here. The first configuration considered is the single stage of the UTRC LSRR. This turbine stage has 22 stators and 28 rotors with an average blade axial chord of 15 cm (6 in.) and axial gap size of 15% average axial chord. Test conditions corresponding to the calculations performed in this study involved ambient air entering the turbine at 23 m/s (75 ft/s) and a mass flowrate of 18 kg/s (40.3 lbm/s). The rotor speed was 410 rpm. The rig was run with and without a turbulence generating grid, and aerodynamic and heat transfer measurements were taken. Although the aerodynamics were not significantly affected by the presence of the grid, the heat transfer profiles measured with the grid in place were substantially different from those measured without the grid. Additional details are given in Refs. 1, 2, and 3.

The second configuration analyzed is the first stage of the SSME HPFTP turbine. This turbine stage has 41 stators and 63 rotors with an average blade axial chord of 2.5 cm (1 in.) and an axial gap size of 0.8 cm (0.33 in.). The turbopump is driven by a gaseous hydrogen and steam mixture which, at full power level, enters the turbine at 226 m/s (741 ft/s), 70 kg/s (154 lbm/s), 1050 K (1900 R), and 37,500,000 N/m^2 (5400 lbf/in^2). The rotor speed is 36,600 rpm.

3. METHOD OF SOLUTION

This analysis was performed by applying an unsteady, viscous, single stage flow formulation to the midspan of the LSRR and HPFTP turbine first stages. The particular code used in this study is ROTOR1.

3.1 CODE DESCRIPTION

ROTOR1 is the two-dimensional (2D) rotor/stator interaction code developed by M.M. Rai (Ref. 4). This code simulates the flow through an axial turbine stage by solving the 2D, unsteady, thin-layer Navier-Stokes equations. It features a factored, iterative, implicit algorithm, an Osher upwind differencing scheme, and a Baldwin-Lomax turbulence model. ROTOR1 employs multiple grids. Each blade is surrounded by a fine O-grid which is overlaid onto a coarse H-grid. The H-grids are patched between blade rows, and the rotor H-grid slides past the stationary stator H-grid in time. ROTOR1 is a single-stage code and assumes that blade rows have an equal blade count. Reference 4 provides a more detailed description of the ROTOR1 methodology.

3.2 BOUNDARY CONDITIONS

The inlet and exit boundary conditions used in this study are the same as those outlined in Ref. 4, so only a brief description will be given here. At the inlet, Riemann invariant $R_1 = u + [2/(\gamma-1)]a$ is fixed and Riemann invariant $R_2 = u - [2/(\gamma-1)]a$ is extrapolated from the interior. The inlet flow angle is set to zero, and the entropy at the inlet is held constant at the freestream value. A constant static pressure is imposed at the exit.

Three different surface temperature conditions were explored: an adiabatic wall, a prescribed wall temperature, and a prescribed heat flux. The no-slip condition and a zero normal pressure gradient, along with one of the temperature conditions, comprise the surface boundary conditions. Reference 4 describes the implementation of these boundary conditions assuming an adiabatic wall. If a nonadiabatic wall is assumed, the wall temperature, T_w, no longer equals T_2, the temperature at the first grid line off the wall. Implementation of the surface boundary conditions assuming a prescribed wall temperature is described below.

To impose no slip, the following equations are required:

$$\Delta\ (\rho_w u_w) = 0$$

$$\Delta\ (\rho_w v_w) = 0 \quad .$$

To impose a zero pressure gradient, solve the energy equation

$$E = \frac{p}{\gamma-1} + \frac{1}{2}\left[\frac{(\rho u)^2}{\rho} + \frac{(\rho v)^2}{\rho}\right]$$

for P and take the normal derivative:

$$\frac{1}{\gamma-1}\frac{\partial p}{\partial n} = \frac{\partial E}{\partial n} - \frac{1}{2}\frac{\partial}{\partial n}\left[\frac{(\rho u)^2}{\rho} + \frac{(\rho v)^2}{\rho}\right] \quad .$$

Setting $\frac{\partial p}{\partial n} = 0$ and expressing the right-hand side in terms of discrete nodal points yields

$$E_2 - E_w = u_w(\rho_2 u_2 - \rho_w u_w) + v_w(\rho_2 v_2 - \rho_w v_w) - \frac{1}{2}(u_w^2 + v_w^2)(\rho_2 - \rho_1) \quad .$$

Applying the no-slip conditions and the time-change operator Δ gives

$$\frac{1}{2}(u_w^2 + v_2^2)\,\Delta\rho_w + \Delta E_w - \frac{1}{2}(u_w^2 + v_w^2)\Delta\rho_2 + u_w\Delta(\rho_2 u_2) + v_w\Delta(\rho_2 v_2) - \Delta E_2 = 0 \quad .$$

To impose a constant blade temperature, use the perfect gas law and apply

$\frac{\partial p}{\partial n} = 0.$

$$\rho_w T_w = \rho_2 T_2$$

Express T_2 in terms of ρ_2, u_2, v_2, and E_2.

$$\rho_2 T_2 = \frac{1}{c_v} [E_2 - u_2(\rho_2 u_2) - v_2(\rho_2 v_2) + \frac{1}{2}(u_2^2 + v_2^2)\rho_2]$$

$$\Delta\rho w - \frac{1}{c_v T_w} [(\frac{u_2^2 + v_2^2}{2})\Delta\rho_2 - u_2\Delta(\rho_2 u_2) - v_2\Delta(p_2 v_2) + \Delta E_2] = 0$$

The equations expressing no-slip, zero normal pressure gradient, and constant blade temperature can be written in matrix form.

$$\begin{bmatrix} 1 & 0 & 0 & 0 \\ 0 & 1 & 0 & 0 \\ 0 & 0 & 1 & 0 \\ \sigma & 0 & 0 & 1 \end{bmatrix} \begin{bmatrix} \Delta(\rho_w) \\ \Delta(\rho_w u_w) \\ \Delta(\rho_w v_w) \\ \Delta(E_w) \end{bmatrix} +$$

$$\begin{bmatrix} -\beta & \delta u_2 & \delta v_2 & -\delta \\ 0 & 0 & 0 & 0 \\ 0 & 0 & 0 & 0 \\ -\sigma & u_w & v_w & -1 \end{bmatrix} \begin{bmatrix} \Delta(\rho_2) \\ \Delta(\rho_2 u_2) \\ \Delta(\rho_2 v_2) \\ \Delta(E_2) \end{bmatrix} = 0$$

where

$$\sigma = (u_w^2 + v_w^2)/2$$

$$\beta = (u_2^2 + v_2^2)/(2c_v T_w)$$

$$\delta = 1/(c_v T_w)$$

The capability to calculate heat transfer was added to ROTOR1. The heat transfer was assumed to be due entirely to conduction, and therefore, Fourier's law of heat conduction was used, i.e.,

$$q'' = -K \frac{\partial T}{\partial n} \quad .$$

Two types of temperature distribution surrounding the blades were considered to approximate the normal derivative of T at the wall. First, the temperature at a blade surface point and at the two closest points along the normal line passing through the surface point was assumed to fit a quadratic polynomial of the form $a+bn+cn^2$, where n is the normal distance from the surface. Next, the temperature distribution was assumed to be linear in n between the boundary point and the first point off the surface. Ideally, in both cases the off-wall point(s) through which the temperature polynomial is fit should lie in the viscous sublayer, i.e., y^+ should be no larger than 10.

3.3 GRID

For both the LSRR and the HPFTP, each O-grid contains 151 circumferential grid lines and 51 radial lines. The stator H-grids have 66 grid lines in the ξ direction and 71 lines in the η direction, while the rotor H-grids contain 76 lines in the ξ direction and 66 lines in the η direction.

As mentioned previously, ROTOR1 assumes that blade rows have an equal blade count; in other words, there is a one to one ratio between stator and rotor blades. However, for the LSRR, the ratio between stator and rotor blades is three to four, and for the HPFTP, the ratio is two to three. In order to produce the appropriate mass flow rate in the calculation with just one stator and one rotor, the stator size must be reduced by 22/28 for the LSRR and 41/63 for the HPFTP, or the rotor size must be enlarged by 28/22 for the LSRR and 64/41 for the HPFTP. Two different grids were generated for the HPFTP, one with a reduced stator and one with an enlarged rotor. No discernible differences in the solutions were found. The HPFTP grid using a reduced stator size is shown in Fig. 1.

4. ROTOR1 ISSUES

Several issues pertaining to ROTOR1 arose while performing the calculations for this study. These issues are discussed in this section.

4.1 REAL GAS VERSUS AIR PROPERTIES

ROTOR1 assumes air to be the turbine's working fluid. This assumption is revealed in the use of gas properties in the code and the use of Sutherland's law to calculate μ. The HPFTP turbine is driven by an H_2/H_2O mixture. The gas properties, such as specific heats, ratio of specific heats, and Prandtl number, can easily be changed from the air values to H_2/H_2O values. However, Sutherland's law is not valid for the HPFTP gas mixture for any Sutherland's constant. To better simulate a non-air flow, a different way of determining the viscosity must be incorporated into ROTOR1.

4.2 SURVIVING INITIAL TRANSIENTS

When ROTOR1 begins its calculations using freestream conditions at all points in the computational domain as an initial approximation to the solution, strong transient pressure waves are generated. These initial waves can be strong enough to cause execution errors in the code. Several methods can be used to survive these transient waves. First, a small time step must be used at the beginning of the calculation. For the configurations in this study, ROTOR1 was run with 2000 iterations per blade pass for the first two blade passes (cycles). This number was decreased (thereby increasing the time step) to 200 iterations per blade pass by the seventh cycle. A way to lessen the strength of the initial transients is to bring the rotor up to speed slowly. ROTOR1 was run for 20 iterations with a rotor speed of zero. The rotor was then brought to full speed gradually over 500 iterations. If the transient waves still cause execution errors (as they did for the HPFTP configuration),

the eddy viscosity can be increased for several blade passes to damp the waves. The eddy viscosity was increased by a factor of 10 at the beginning of the calculation for the HPFTP. The viscosity was gradually decreased to its appropriate value over three blade passes.

4.3 ITERATIVE PROCEDURE

For some configurations and conditions, the solution to which ROTOR1 converges is inappropriate. Because a Riemann invariant, not actual values, is fixed at the inlet, the inlet values may change during the calculation. A solution is then generated based on inlet conditions different from the desired conditions. In order to produce a solution with the correct inlet conditions, an iterative procedure is necessary. ROTOR1 is first run to convergence using the correct values of inlet Mach number and velocity. The converged value of inlet velocity is then compared with the correct value. If the velocities differ, the inlet Mach number is adjusted in the following manner:

$$M_{new} = M_{old} + \frac{u_{input} - u_{converged}}{a_{converged}} .$$

The new inlet Mach number, M_{new}, is then input into ROTOR1, becoming M_{old}, and the code is run until a periodic solution is obtained. Again, the converged inlet velocity is compared to the correct value, and the Mach number is adjusted if necessary. This procedure is repeated until the converged values of Mach number and velocity match the correct values. For the LSRR, the converged inlet Mach number and velocity matched the input values in the first run; no adjustments were needed. Calculations for the HPFTP were performed four times to obtain the correct inlet values.

5. RESULTS AND DISCUSSION

Calculations were performed on the Cray X-MP 416 computer at Marshall Space Flight Center. A ROTOR1 calculation starting from freestream conditions requires six CPU hours to reach periodicity and $2.1 \cdot 10^6$ words of core memory plus $4.1 \cdot 10^6$ words of solid state storage device (SSD).

Results generated using the modified ROTOR1 code are presented here. The results are divided into two classifications, aerodynamic and thermal. Aerodynamic results are shown in the form of instantaneous contour plots, unsteady pressure envelopes, and blade pressure coefficients. The thermal results are presented in terms of heat transfer coefficients or Stanton numbers.

5.1 AERODYNAMIC RESULTS

Plots of calculated and experimentally measured pressure coefficients, defined as

$$C_p = (p - p_{To}) \Big/ (\tfrac{1}{2} \rho_o \omega^2)$$

are shown in Figs. 2 and 3 for the LSRR. These C_p profiles represent time-averaged values p, p_{To}, and ρ_o. The agreement between the prediction and test data is excellent and consistent with results reported in Ref. 4. Pressure coefficients calculated for the SSME HPFTP are shown in Figs. 4 and 5.

Figures 6 through 9 show the unsteady pressure envelopes for the LSRR and HPFTP. In both turbines, the effects of rotor/stator interaction, shown by the variations in pressure amplitudes, are experienced significantly by the rotor. Effects are also seen on the LSRR stator due to the narrow axial gap. The larger axial spacing in the HPFTP minimizes the effects of the blade

interaction communicated upstream in the turbine. Figures 10 through 12 show instantaneous contours for the HPFTP configuration. Figure 13 illustrates the flowfield unsteadiness which can be characterized by a ROTOR1 calculation. This plot shows the migration of the stator wake through the rotor passage.

5.2 THERMAL RESULTS

Stanton numbers for the LSRR were calculated using two different expressions. One definition is consistent with the measured Stanton numbers reported in Refs. 2 and 3, i.e.,

$$St = \frac{q''}{\rho_e U_e c_p (T_w - T_{To})} .$$

This definition poses a problem. As q" is not dependent upon $T_w - T_{To}$, but instead on $T_a - T_w$ (Ref. 5), nondimensionalization by $T_w - T_{To}$ yields a Stanton number dependent of T_w. The question of what wall temperature is the appropriate temperature to prescribe at the blade surface as a boundary condition becomes an important issue. Figure 14 shows calculated Stanton number for the LSRR rotor with three different wall temperatures. Three different Stanton number profiles result.

The Stanton number was redefined to remove the wall temperature dependence:

$$St = \frac{q''}{\rho_e U_e c_p (T_a - T_w)} .$$

Figures 15 and 16 show blade-temperature independent Stanton numbers for the LSRR. Also shown are predictions resulting from specification of a constant heat flux, which are seen to be low in comparison to the prescribed wall temperature results. Experimental data are also shown. Comparison of the stator profiles shows the prediction to be essentially laminar on the pressure surface where the calculated profile shape resembles the grid-out measurements. Calculations for the stator suction surface fail to correctly predict the transition

point or the profile shape. The calculated rotor pressure surface appears low and flat as compared with the experimental data. The shape of the suction surface profile, however, closely matches the shape of the grid in measurements, although the magnitude of the predicted profile is lower than that measured.

Figures 17 and 18 show Stanton numbers for the HPFTP. Also shown on these plots are Stanton numbers calculated with a more conventional steady inviscid code, STAN5 (Ref. 6). A discrepancy between the ROTOR1 and STAN5 results is apparent. This could be due to the ROTOR1 assumption of air as the working fluid in its calculation of μ. STAN5 incorporates real gas properties.

7. CONCLUSIONS

A numerical study of the unsteady aerodynamic and thermal environment associated with axial turbine stages was conducted, using the code ROTOR1. ROTOR1 was applied to two different turbine stages: the first stage of the UTRC LSRR and the SSME HPFTP turbine first stage.

ROTOR1 is an effective tool with which to characterize the unsteady nature of flows through axial turbines. Instantaneous contours can be generated for any time within a blade pass, and unsteady flow features can be tracked through time. Time-averaged quantities can also be calculated with ROTOR1. Time-averaged pressure distributions calculated with ROTOR1 compare well with the experimental data. Qualitatively, the heat transfer profiles predicted for the LSRR exhibit reasonable agreement with the data, except on the stator suction surface where ROTOR1 fails to correctly predict the transition location and profile shape. The magnitude of the Stanton numbers is somewhat low, particularly when a constant heat flux boundary condition is imposed in ROTOR1. The ROTOR1-predicted heat transfer for the SSME HPFTP does not compare favorably with the conventional STAN5 prediction. The discrepancy is believed to be due to the ROTOR1 assumption of air as the working fluid for the viscosity calculation. This assumption yields erroneous heat transfer results for turbines that are not air driven.

REFERENCES

1. Dring, R.P. et al., "The Effects of Inlet Turbulence and Rotor/Stator Interactions on the Aerodynamics and Heat Transfer of a Large-Scale Rotating Turbine Model, Vol. IV: Aerodynamics Data Tabulation," NASA CR 179469, November 1987.

2. Dring, R.P. et al., "The Effects of Inlet Turbulence and Rotor/Stator Interactions on the Aerodynamics and Heat Transfer of a Large-Scale Rotating Turbine Model, Vol. I: Final Report," NASA CR 4079, May 1986.

3. Dring, R.P. et al., "The Effects of Inlet Turbulence and Rotor/Stator Interactions on the Aerodynamics and Heat Transfer of a Large-Scale Rotating Turbine Model, Vol. II: Heat Transfer Data Tabulation, 15% Axial Spacing." NASA CR 179469, May 1986.

4. Rai, M.M., "Navier-Stokes Simulations of Rotor/Stator Interactions Using Patched and Overlaid Grids," Journal of Propulsion and Power, Vol. 3, No. 5, September 1987, pp. 387-396.

5. White, F.J., Viscous Fluid Flow. McGraw-Hill, New York, 1974, pp. 269-271.

6. Crawford, M.W. and W.M. Kays, "STAN5 - A Program for Numerical Computation of Two-Dimensional Internal and External Boundary Layer Flows," NASA CR-2742, December 1976.

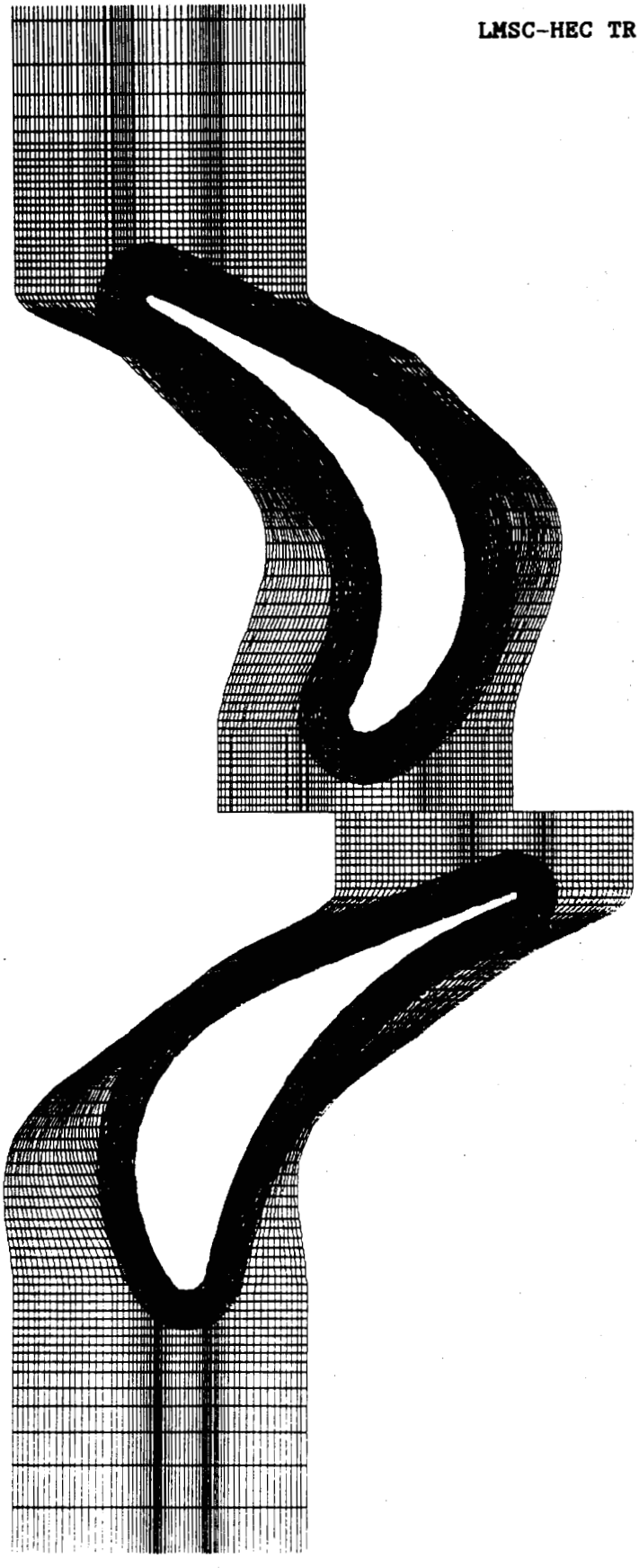

Fig. 1 SSME HPFTP Turbine First Stage Grid

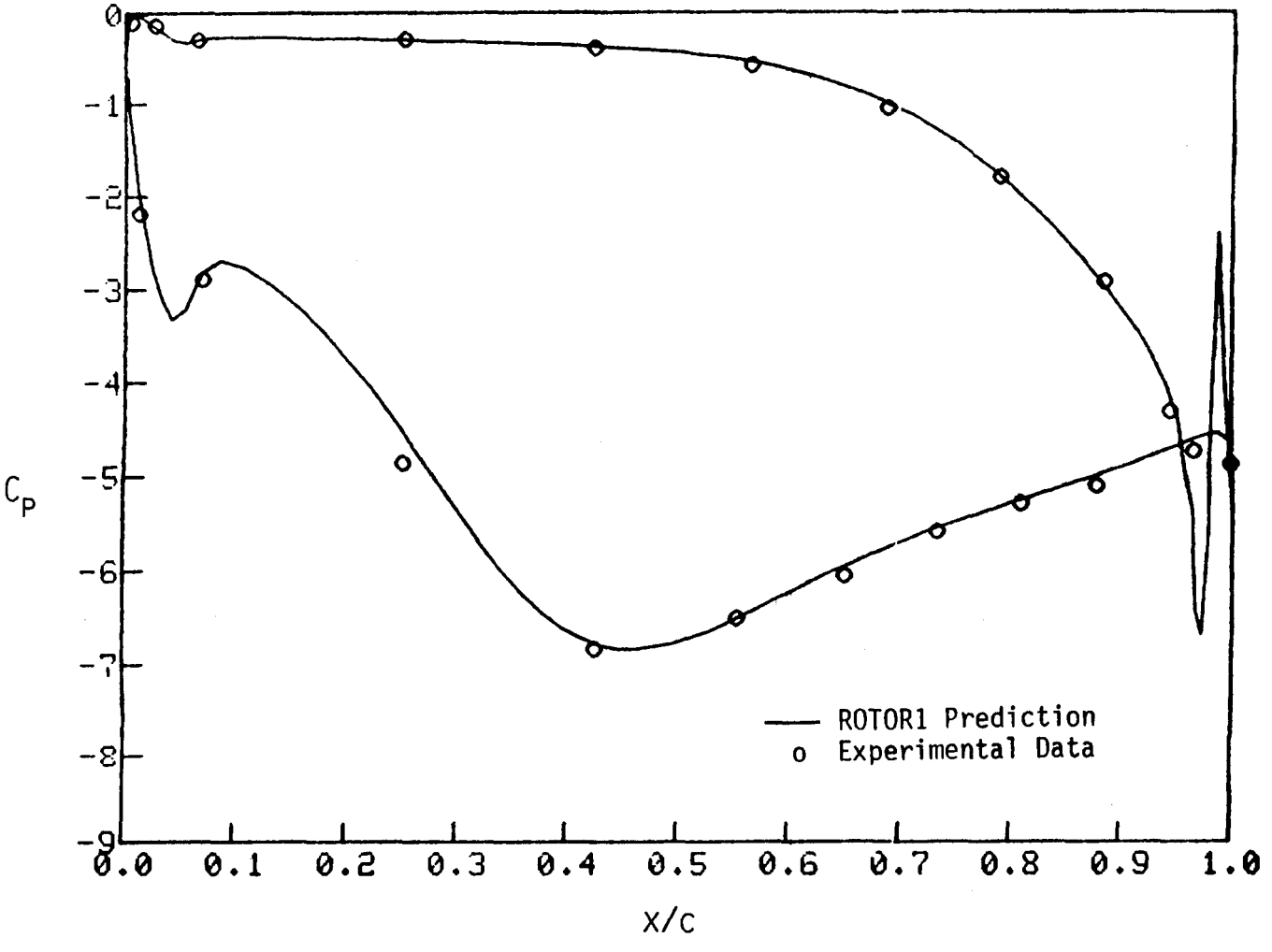

Fig. 2 Pressure Distribution on the LSRR First Stator

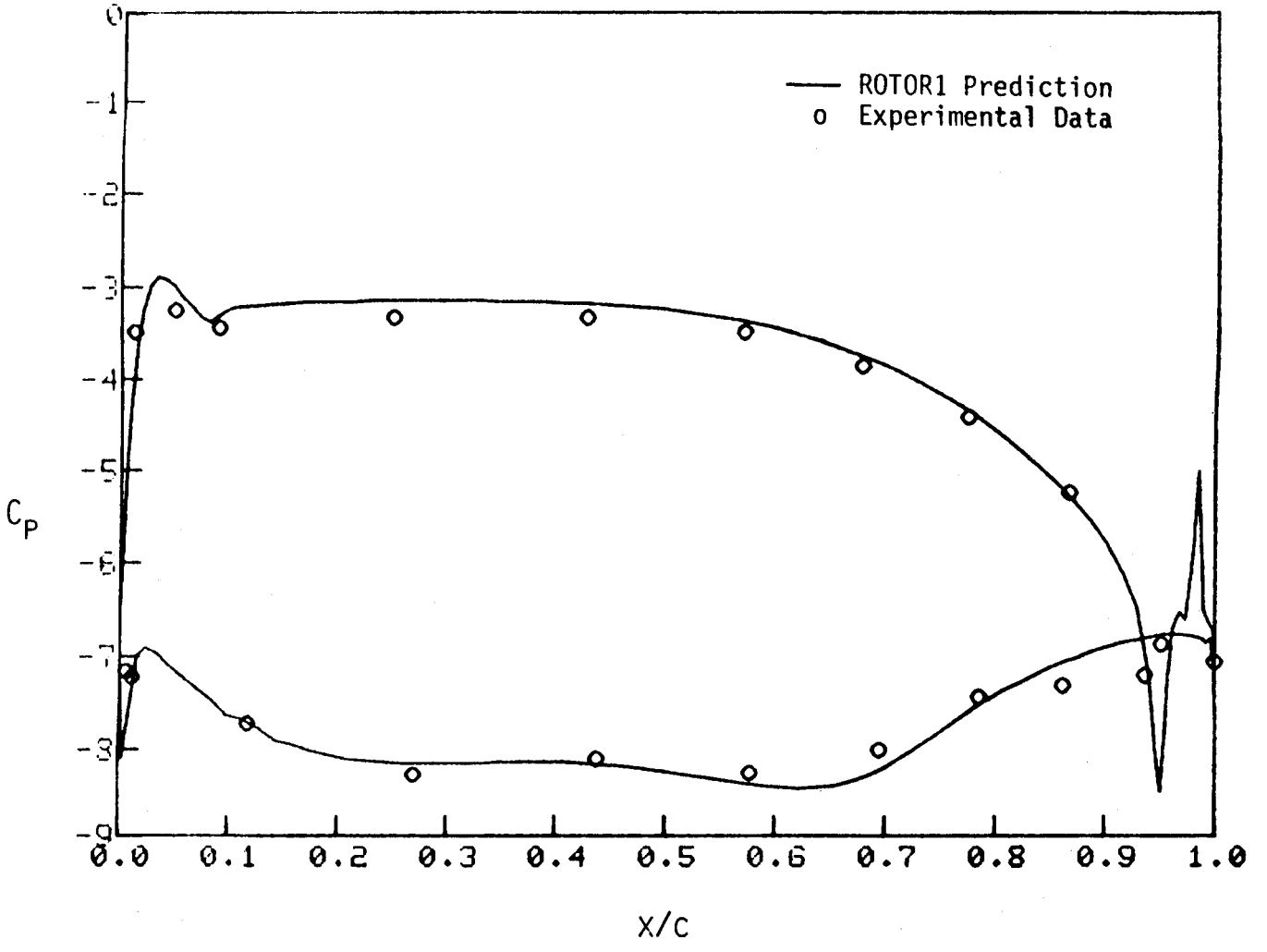

Fig. 3 Pressure Distribution on the LSRR Rotor

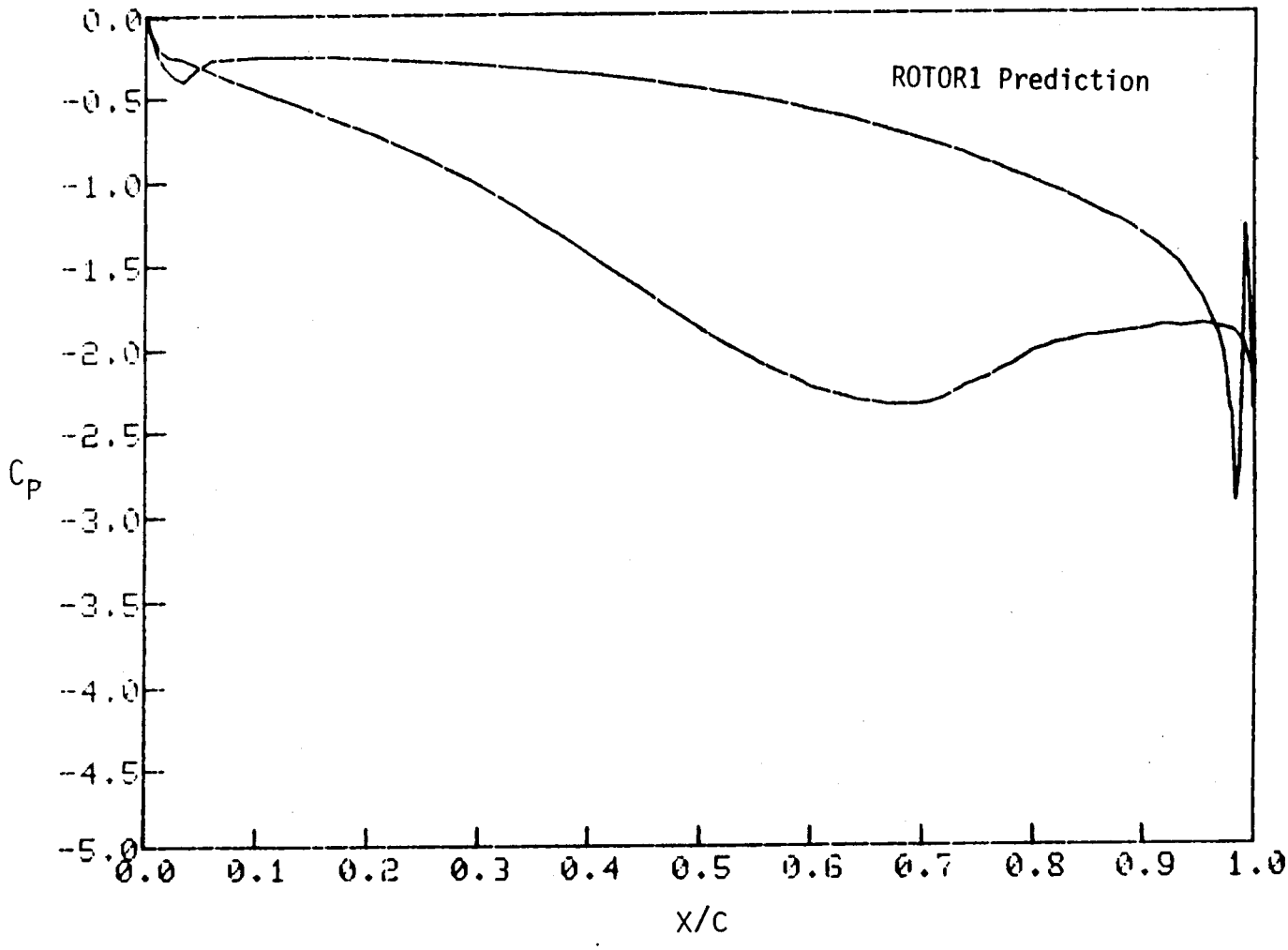

Fig. 4 Pressure Distribution on the SSME HPFTP First Stator

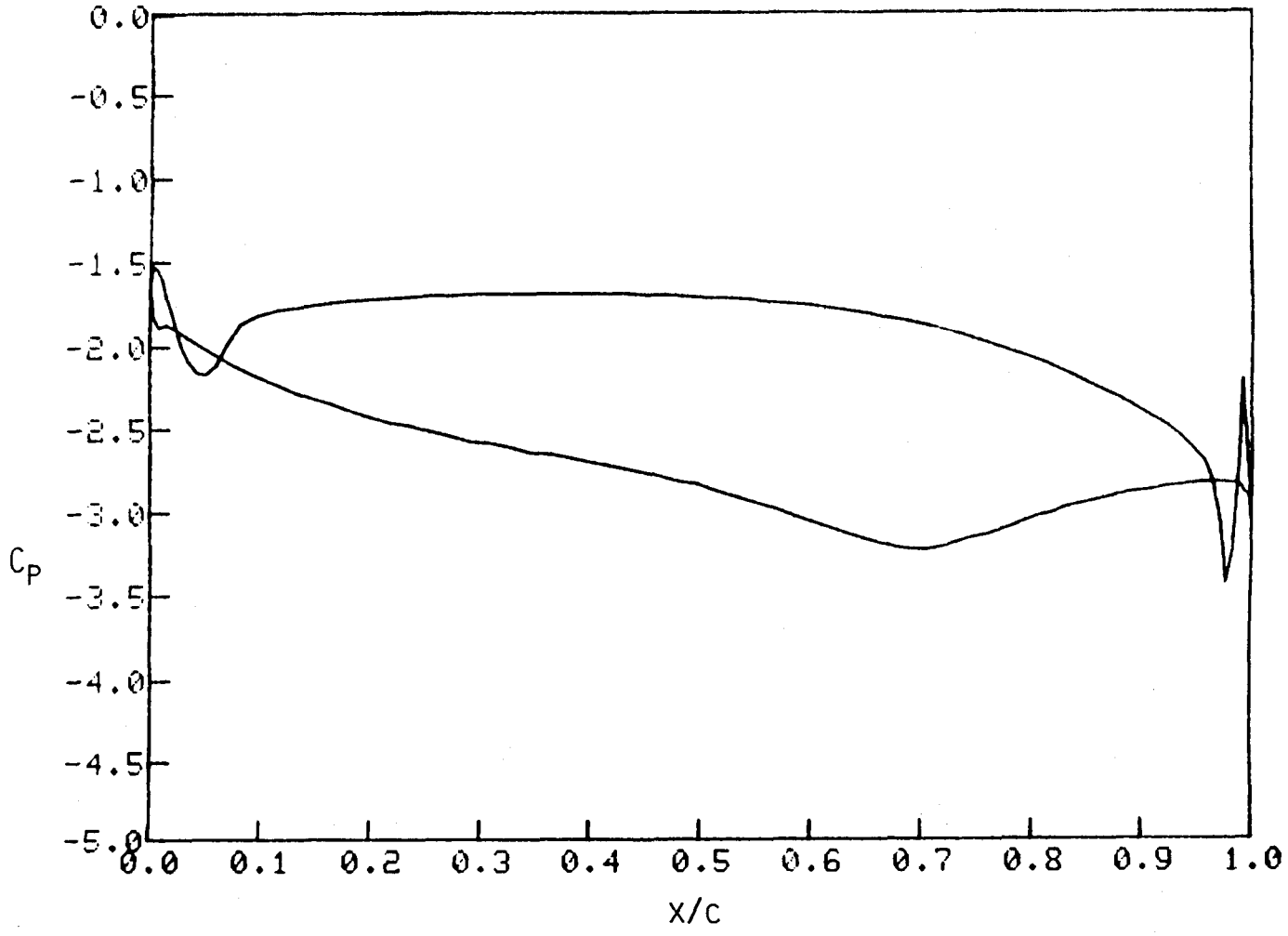

Fig. 5 Pressure Distribution on the SSME HPFTP First Rotor

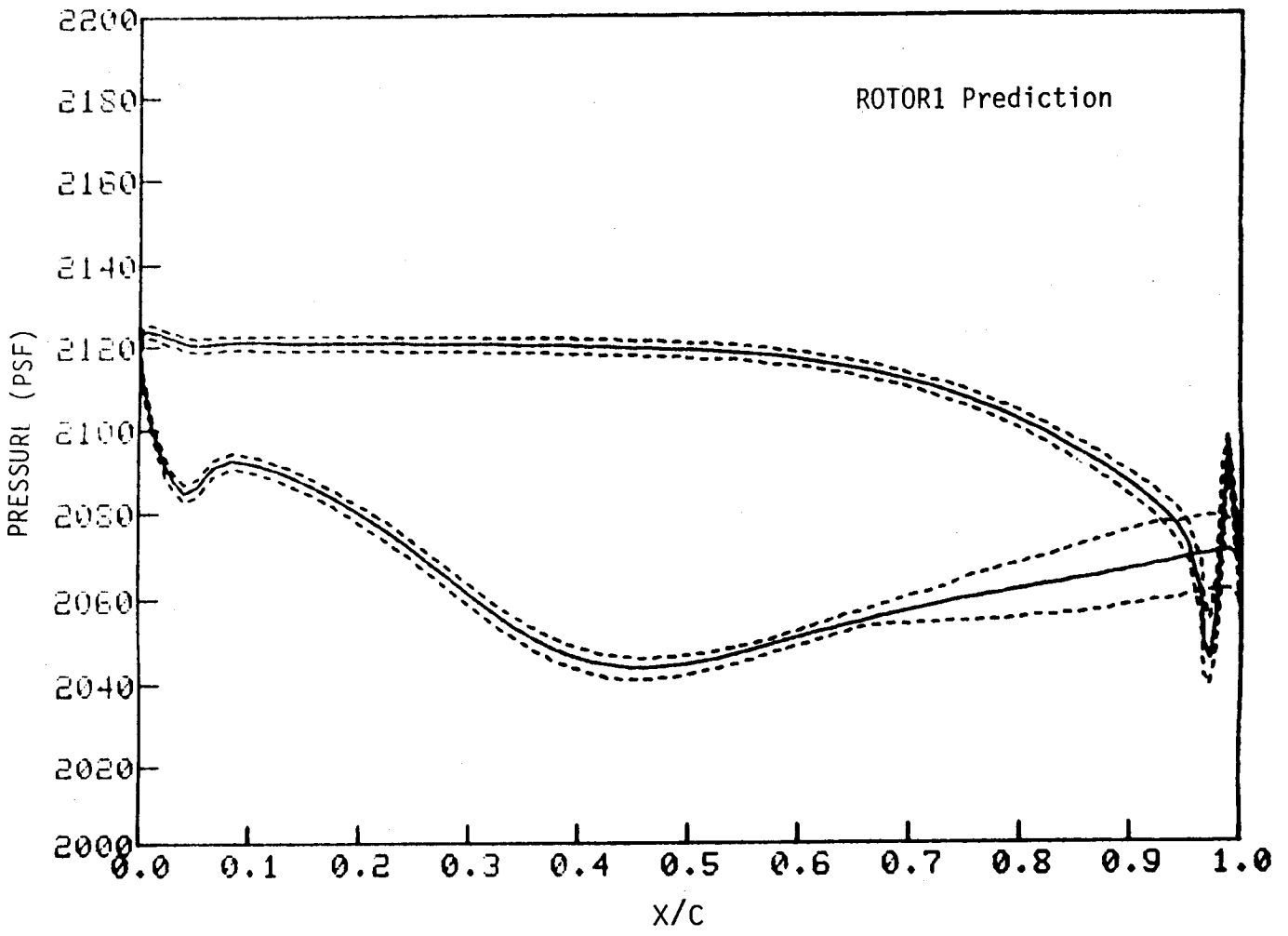

Fig. 6 Unsteady Pressure Envelope of the LSSR First Stator

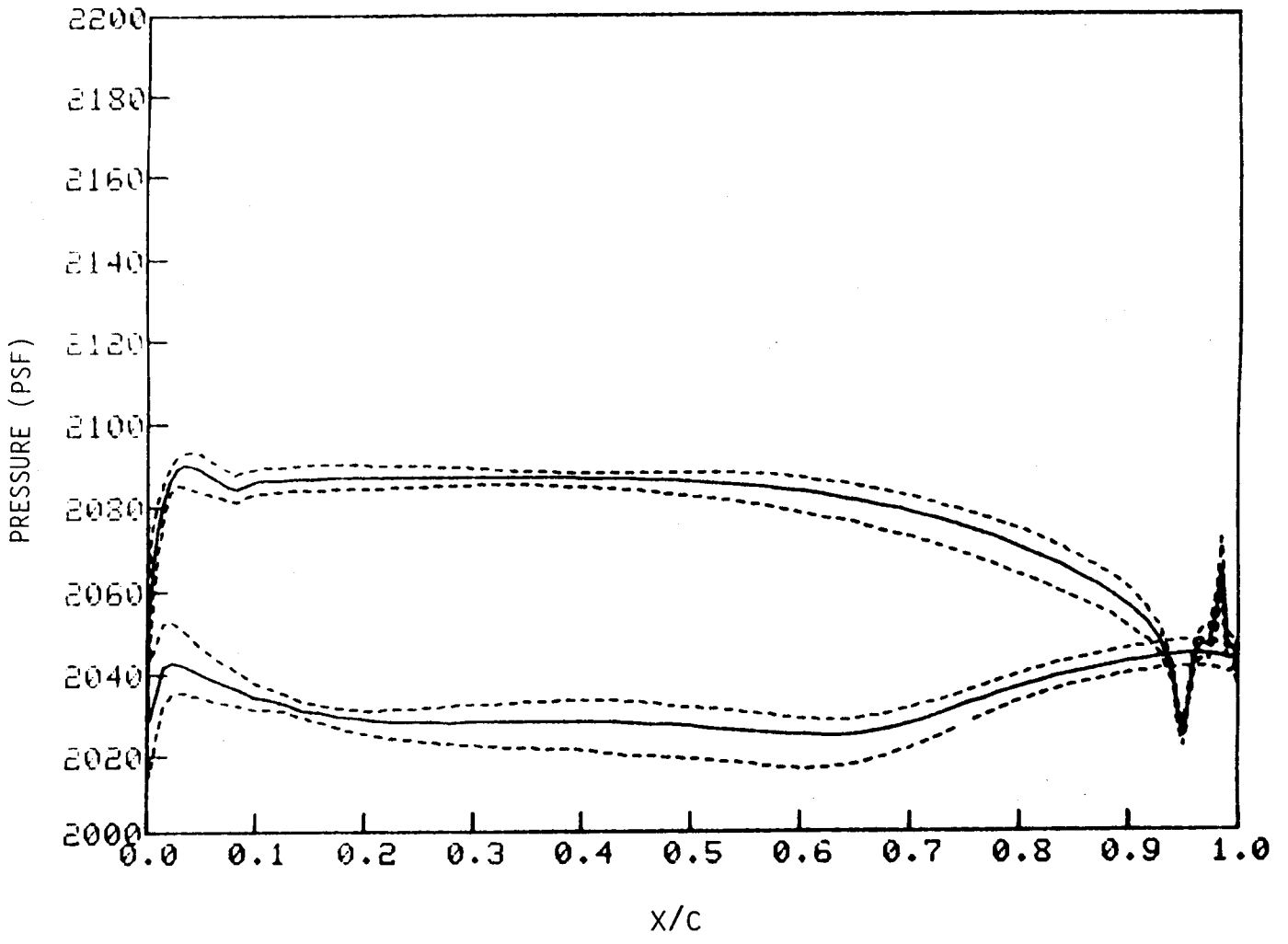

Fig. 7 Unsteady Pressure Envelope of the LSSR Rotor

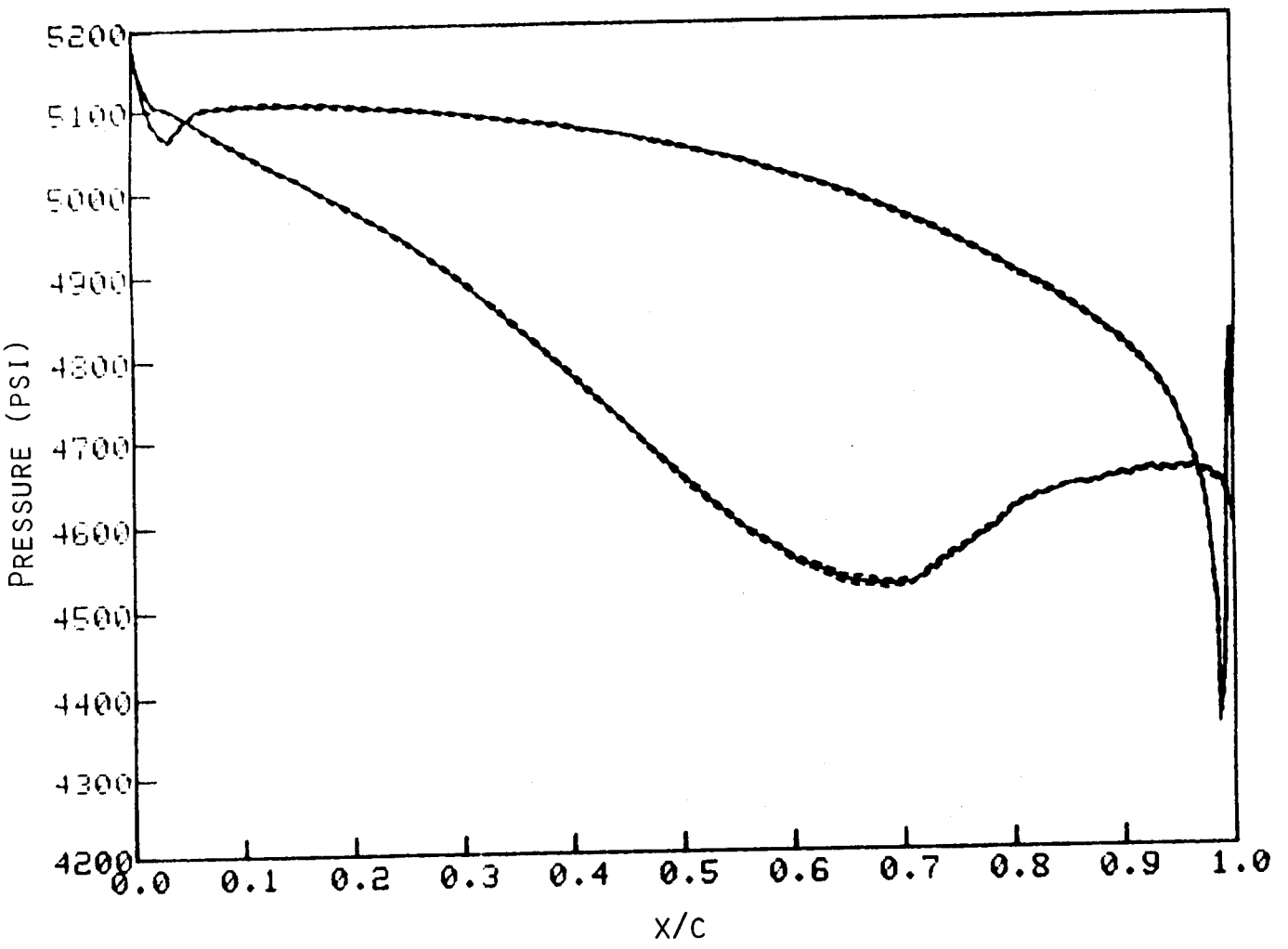

Fig. 8 Unsteady Pressure Envelope of the SSME HPFTP First Stator

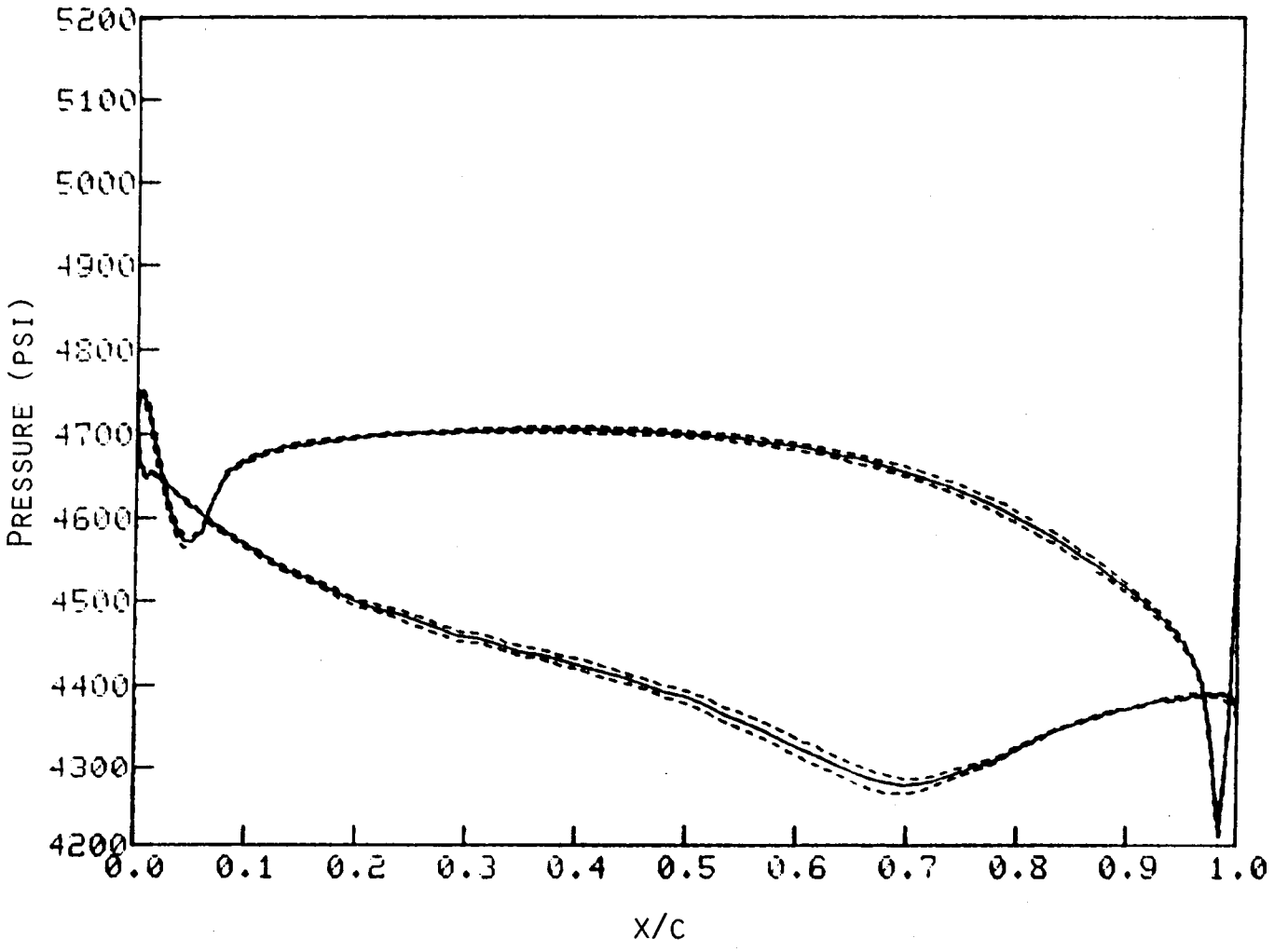

Fig. 9 Unsteady Pressure Envelope of the SSME HPFTP First Rotor

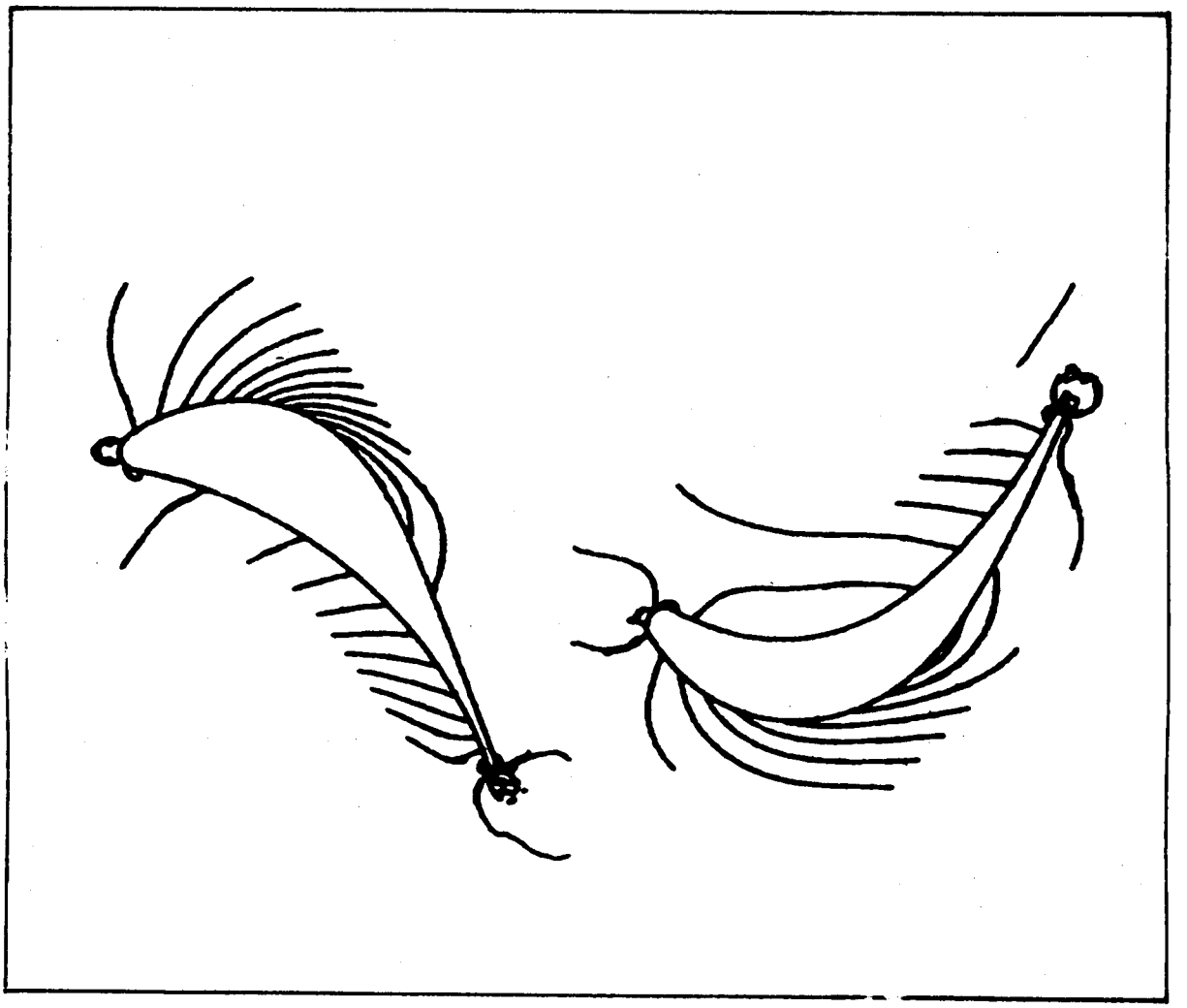

Fig. 10 Instantaneous Pressure Contours for the SSME HPFTP Turbine

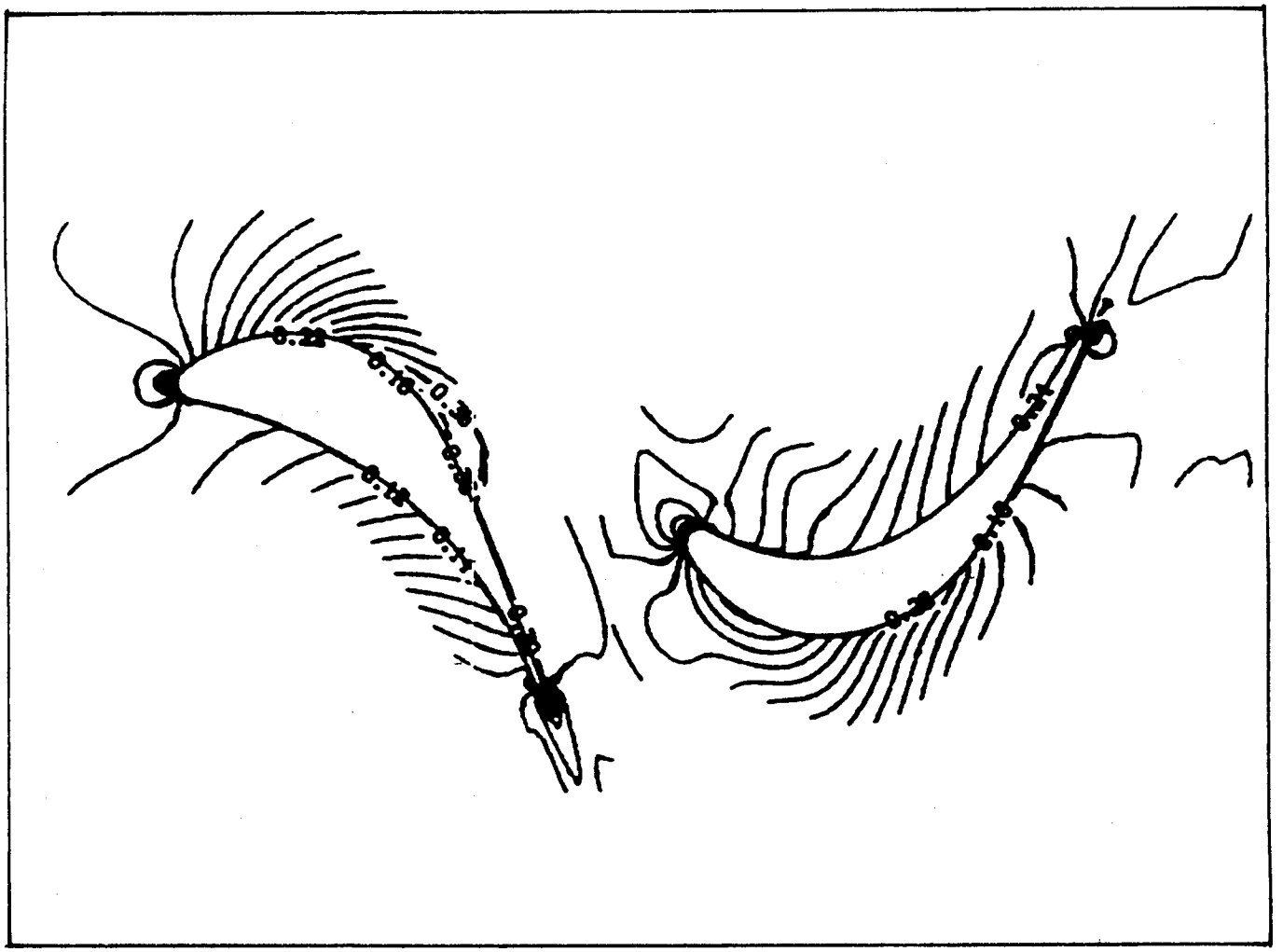

Fig. 11 Instantaneous Mach Contours for the SSME HPFTP Turbine

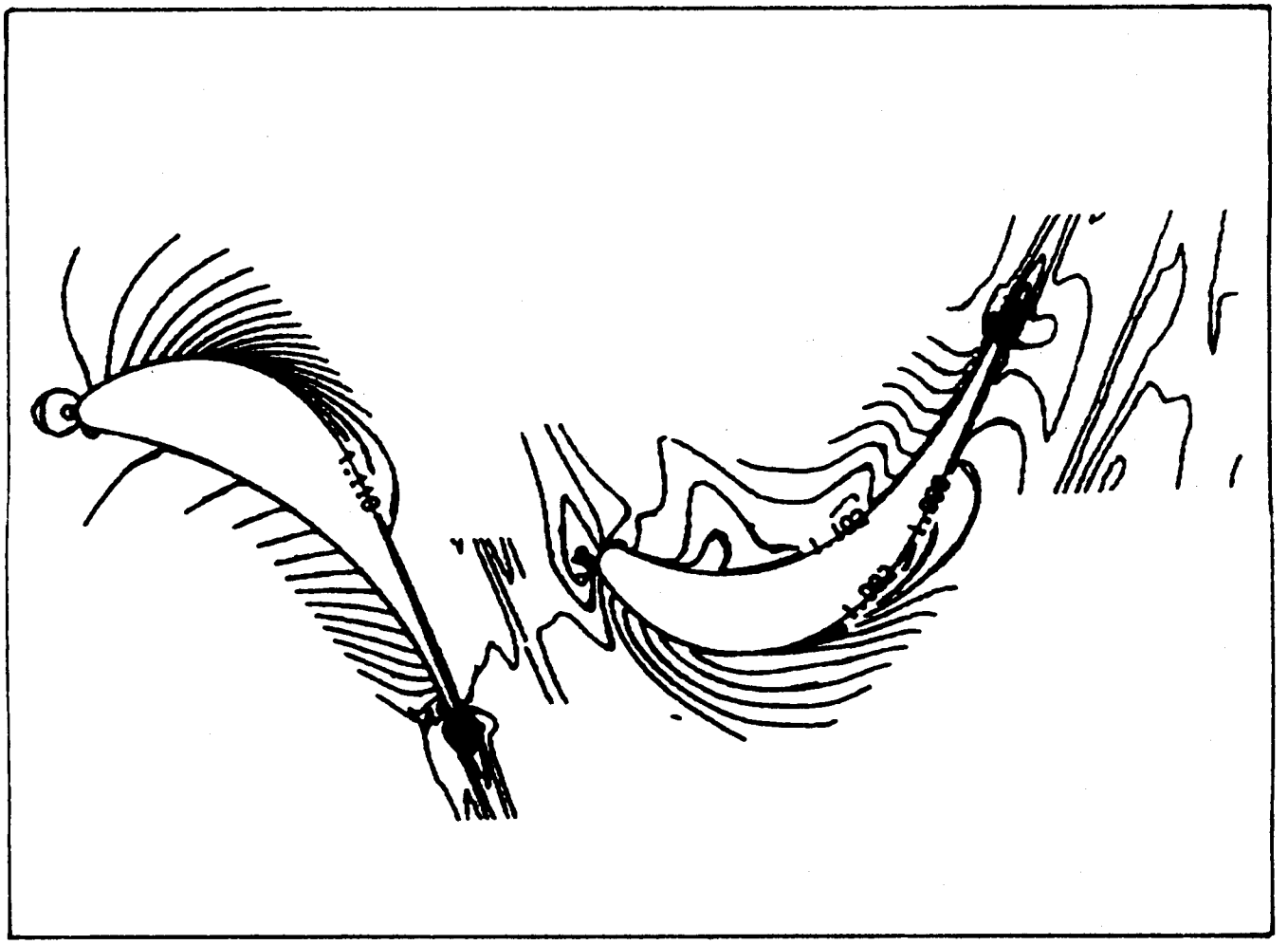

Fig. 12 Instantaneous Temperature Contours for the SSME HPFTP Turbine

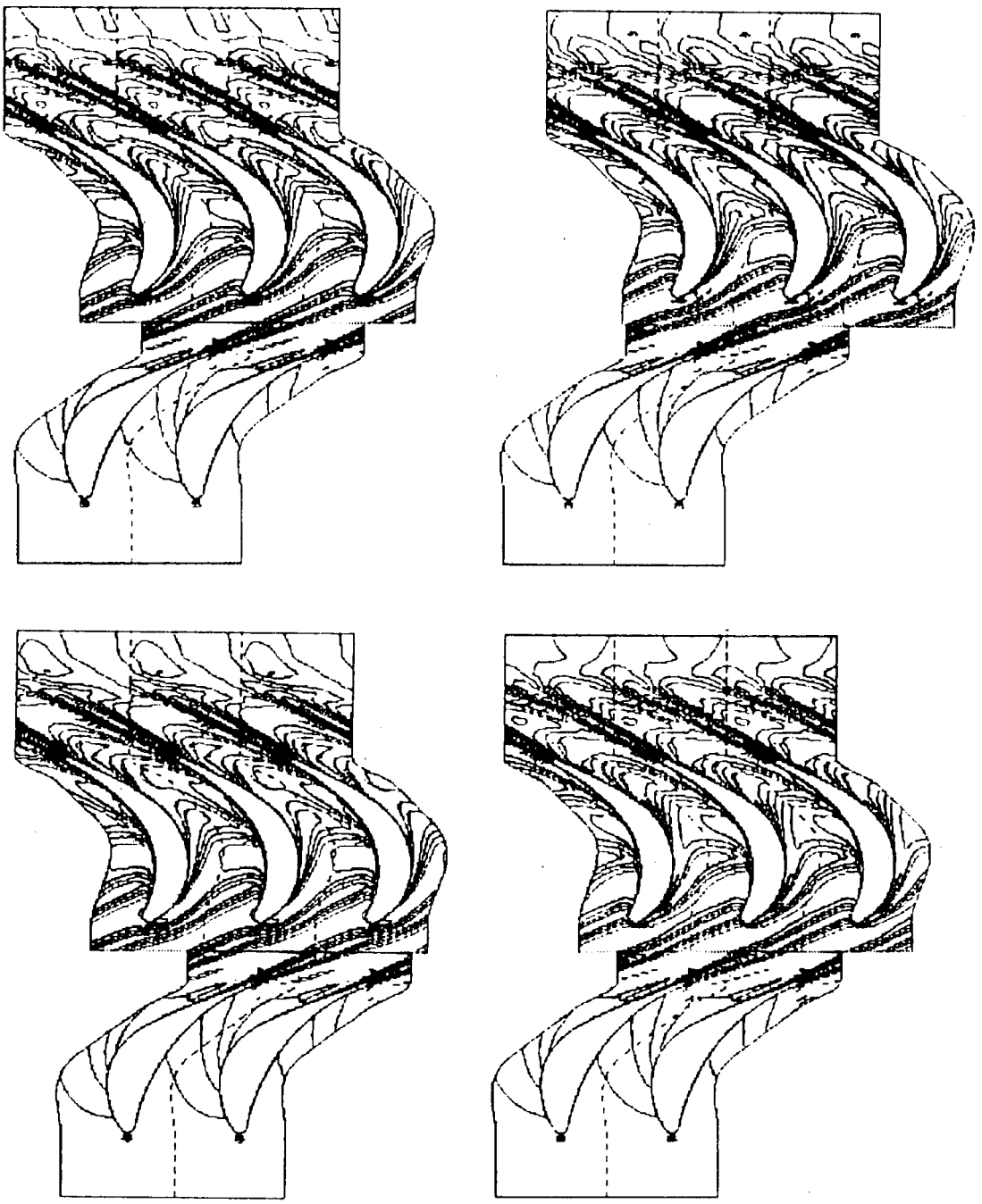

Fig. 13 Instantaneous Entropy Contours at Four Different Times for the SSME HPFTP Turbine (Graphics by D. Good and J. Ruf of NASA-Marshall Space Flight Center)

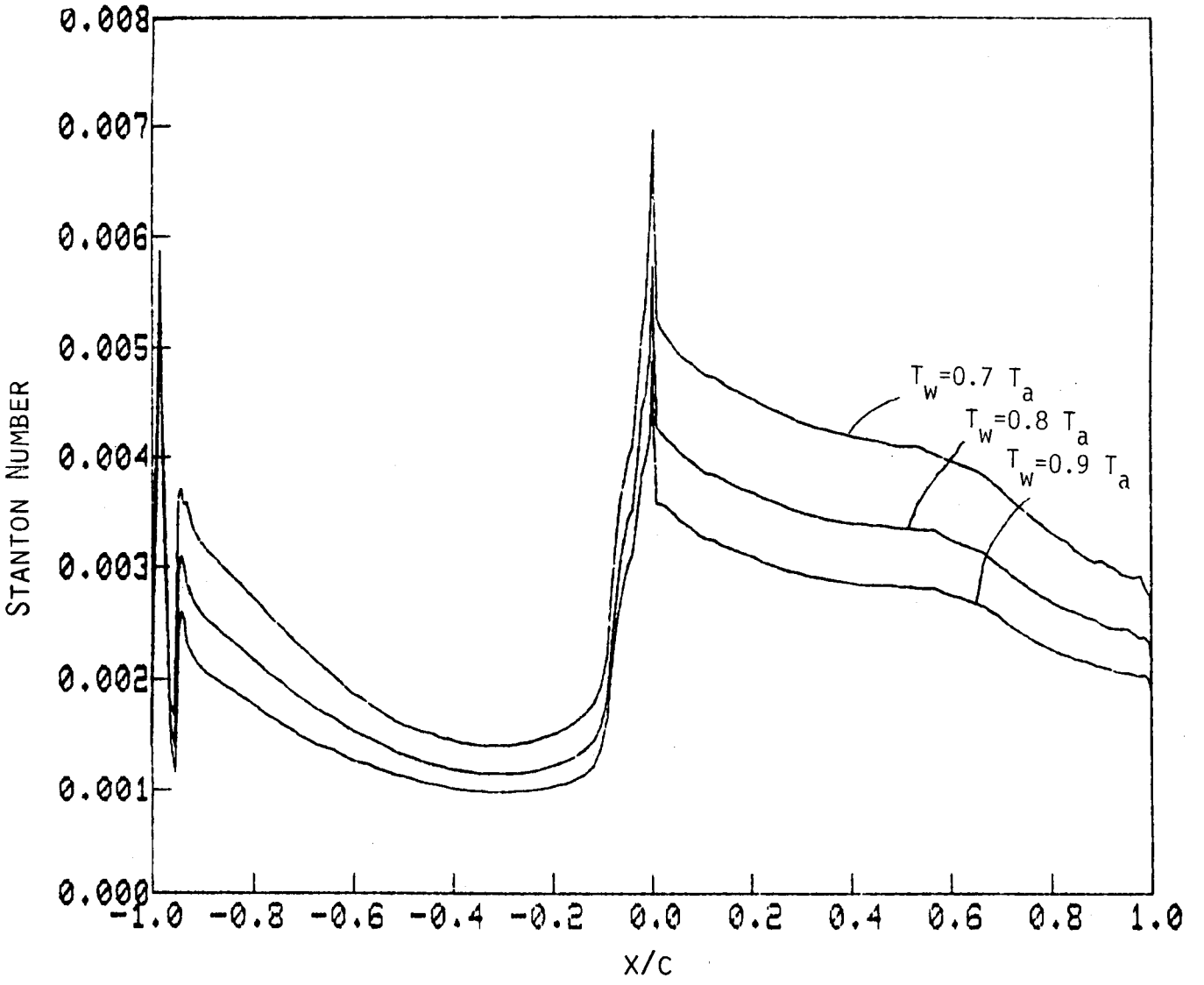

Fig. 14 Effects of Wall Temperature on Stanton Number

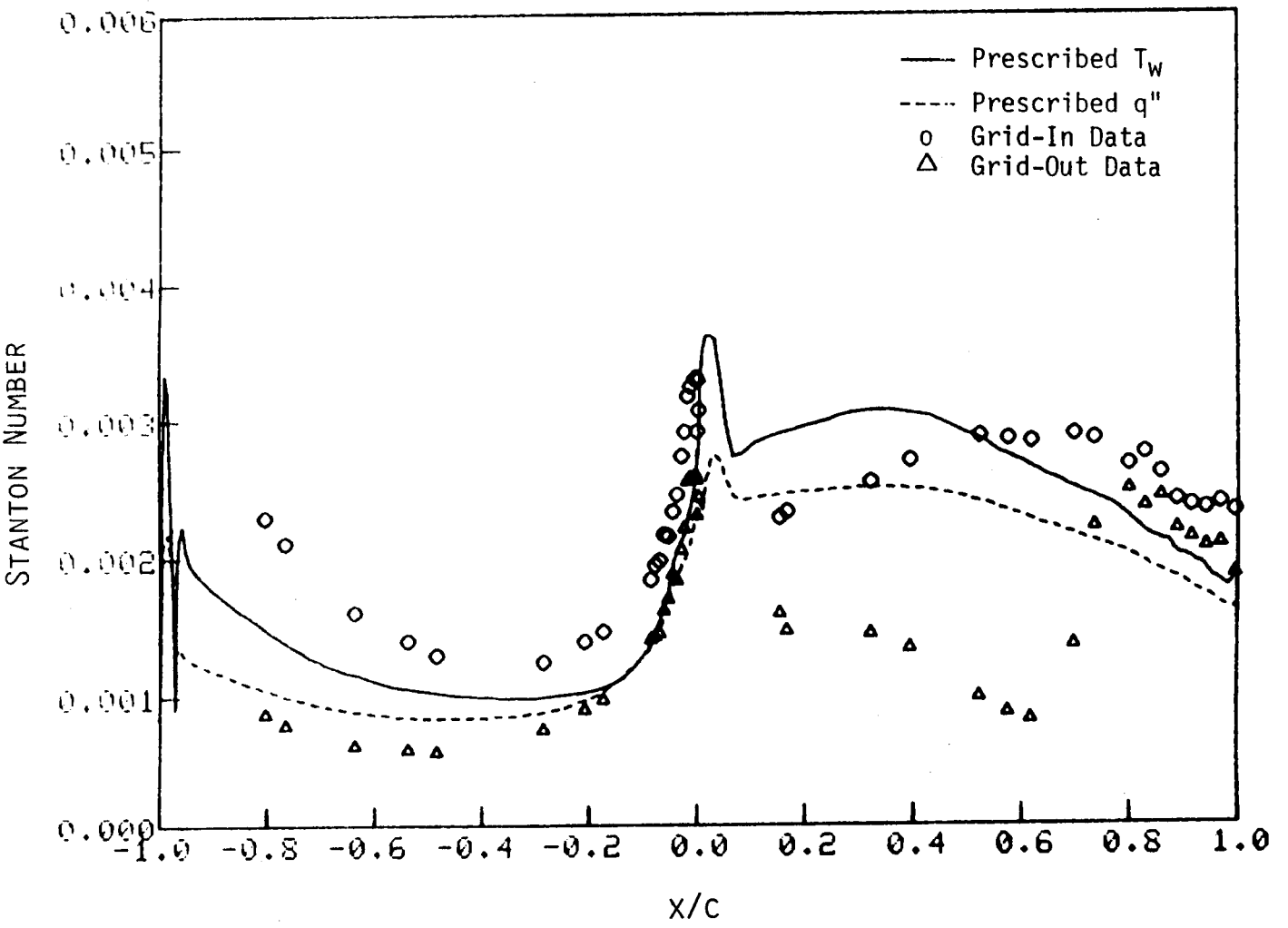

Fig. 15 Comparison of ROTOR1 Predicted and Experimental Heat Transfer for the LSRR First Stator

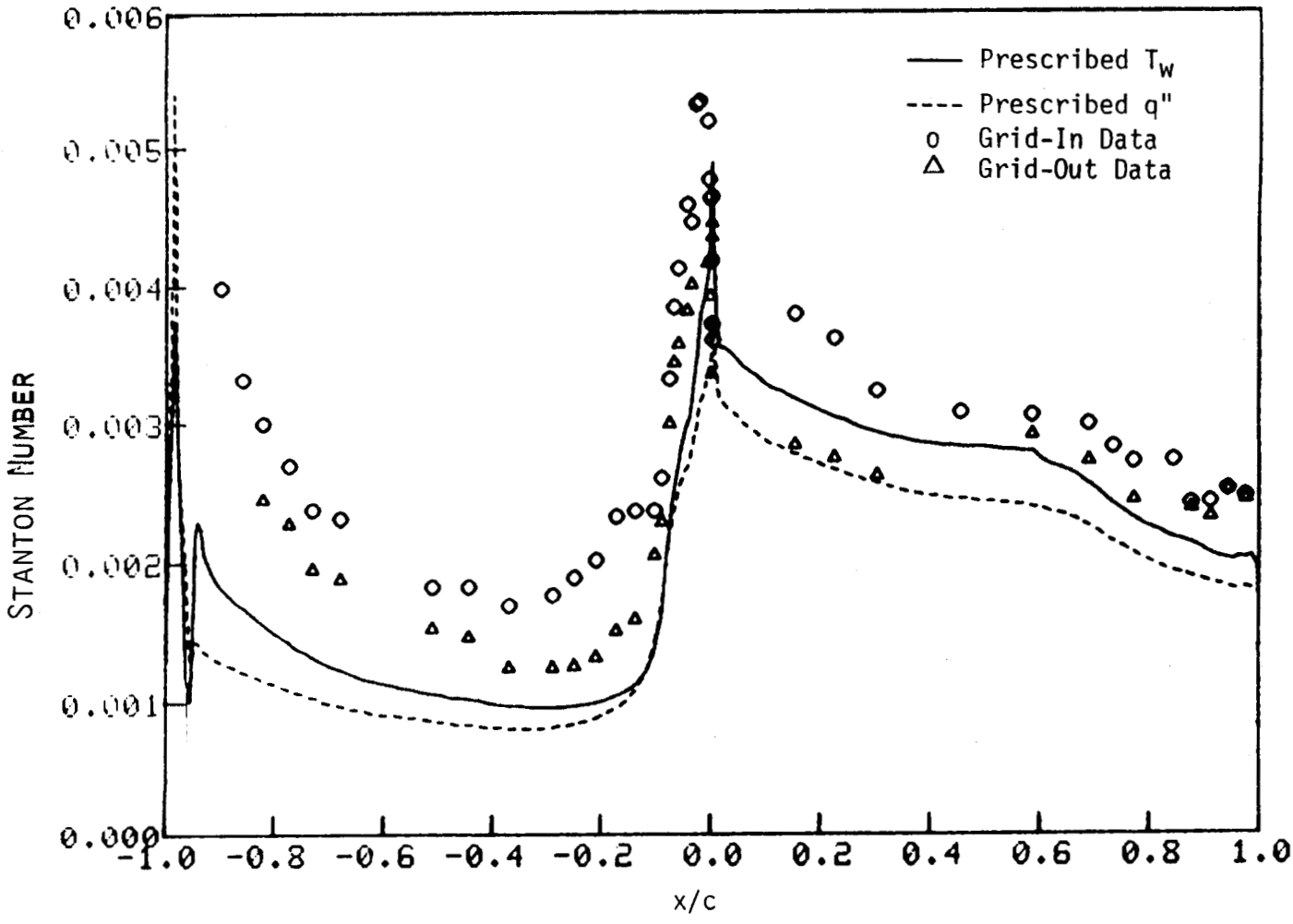

Fig. 16 Comparison of ROTOR1 Predicted and Experimental Heat Transfer for the LSRR Rotor

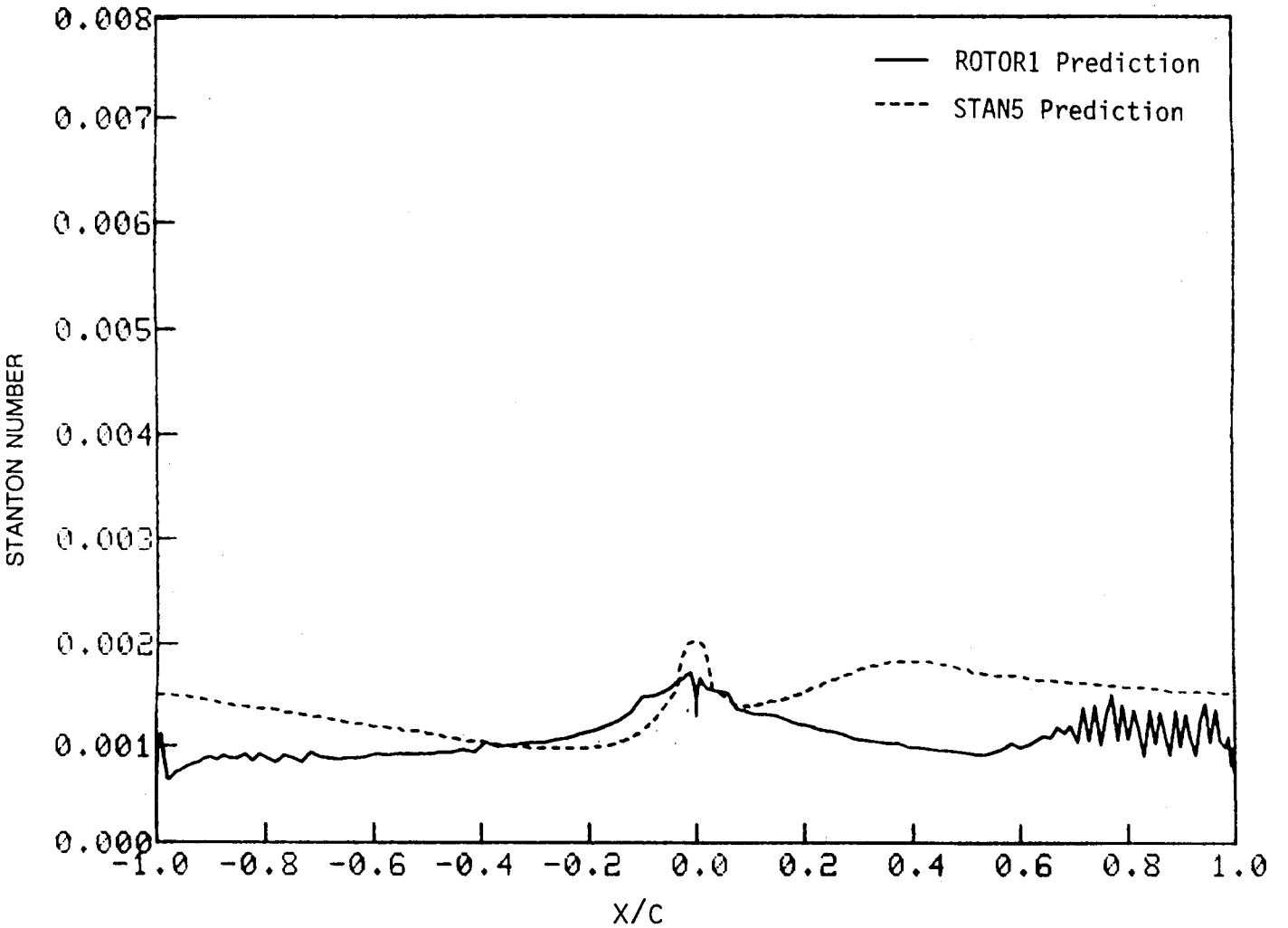

Fig. 17 Comparison of ROTOR1 and STAN5 Heat Transfer Predictions for SSME HPFTP First Stator (STAN5 Calculation by H. McConnaughey of NASA-Marshall Space Flight Center)

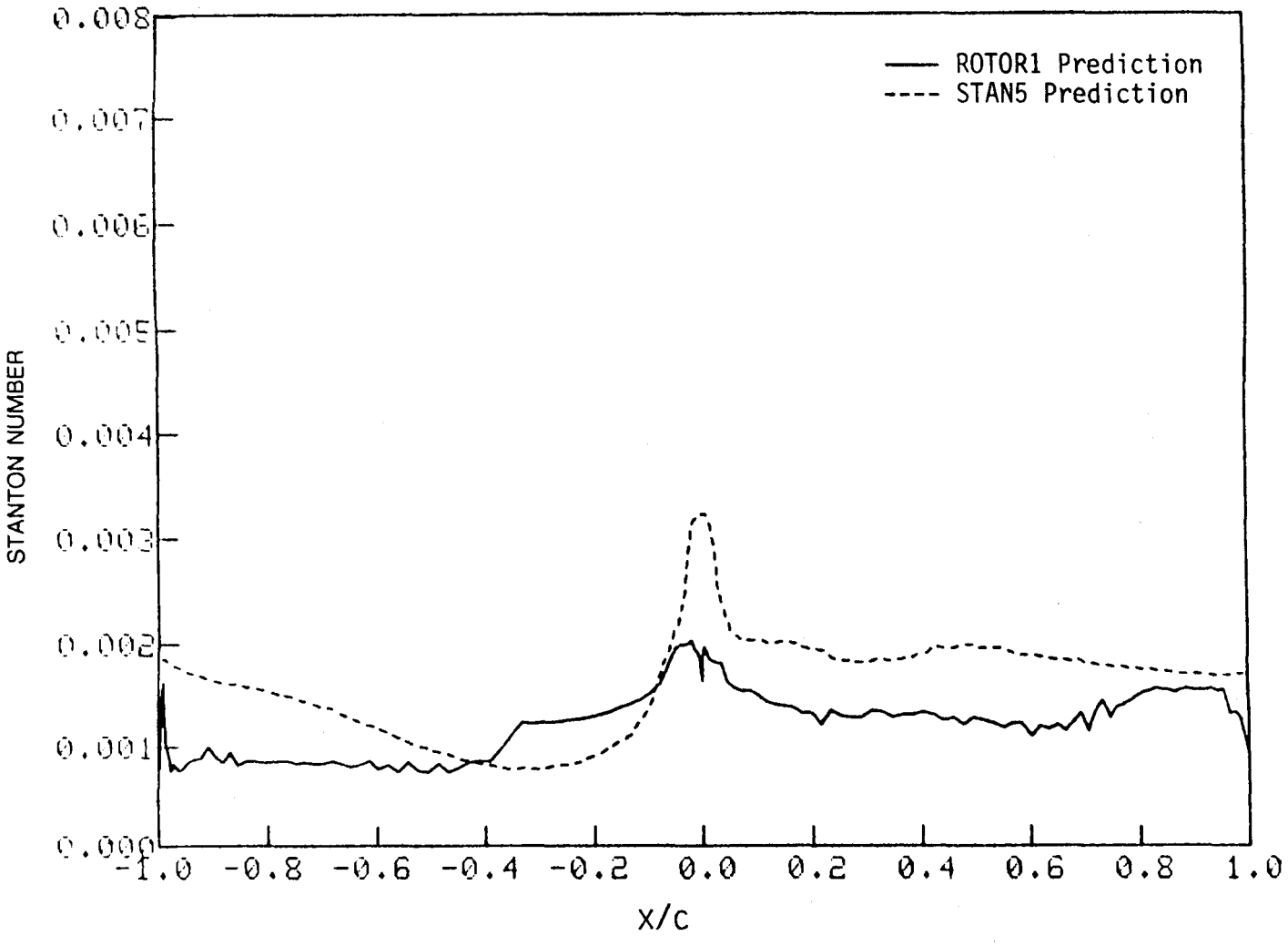

Fig. 18 Comparison of ROTOR1 and STAN5 Heat Transfer Predictions for HPFTP First Rotor (STAN5 Calculation by H. McConnaughey of NASA-Marshall Space Flight Center)